

Oxygen Sensors for Industrial Application

J. N. Nhangá¹




¹Department of Metallurgical and Materials Engineering, Faculty of Engineering, University of Porto, Rua Dr. Roberto Frias, 4200-465 Porto, Portugal (up201708830@edu.fe.up.pt) ORCID [0000-0001-9813-2172](https://orcid.org/0000-0001-9813-2172)

Abstract

The present work aimed to study a family of solid ceramic electrolytes based on magnesium oxide doped zirconium oxide, usually identified as Mg-PSZ (zirconia partially stabilized with magnesia), used in the manufacture of oxygen sensors for molten metals. A set of electrolytes was prepared by mechanical (milling) and thermal (sintering) processing, varying the composition in magnesia and the cooling rate from the sintering temperature. These two parameters are essential in terms of phase composition and microstructure of Mg-PSZ, determining the behavior of these materials. The structural and microstructural characterization was done by means of X-ray diffraction (XRD). The electrical properties were analyzed by impedance spectroscopy in air. In general, the results obtained from various concentrations of dopant, different cooling rates and the same sintering step condition showed an increased conductivity for samples with predominance of high temperature stable phases (tetragonal and cubic).

Author Keywords. Partially Stabilized Zirconia, Oxygen Sensors, Impedance Spectroscopy, X-ray Diffraction, Scanning Electron Microscopy.

Type: Research Article

 Open Access  Peer Reviewed  CC BY

1. Introduction

The development of solid electrolytes based on materials such as zirconium oxide has aroused interest due to its high ionic conductivity over wide temperature ranges and partial pressure of oxygen. Among the most important applications of these materials, we highlight the oxygen sensors for molten metal. For this application, the solid electrolyte must comply with a series of requirements, such as high densification (> 92% of the theoretical in order to prevent the passage of gases through the interior of the electrolyte), purely ionic conductivity and great resistance to thermal shock. These properties are strongly dependent on the phased composition and microstructure, both conditioned by the chemical composition and thermal path ([Grzebielucka et al. 2010](#)).

In view of this application and the existing knowledge about the most promising candidates for this function (zirconium oxide as the base material and magnesium oxide as a dopant), the materials tested in this work were prepared based on a ceramic processing method, from the precursor oxides, using mainly different compositions and profiles for sintering (cooling) ([Rezaei et al. 2006](#)).

2. State-of-the-Art

Zirconium oxide, of chemical formula ZrO_2 , commonly known as zirconia, has several technological applications in refractories, structural ceramics, biomaterials, oxygen sensors and fuel cells, due to your excellent properties chemical, mechanical, electrical and thermal. These applications range from room temperature (for example, in dental crowns) to

temperatures above 1500 °C (in sensors for molten metals) (Grzebielucka et al. 2010). Pure zirconia generally has three different structural shapes during heating to its melting temperature (Figure 1). Under normal conditions of temperature and pressure it presents the monoclinic structure (m-ZrO₂), with the ion Zr⁴⁺ surrounded by seven anions, that is, with coordination 7. As the temperature rises, and close to 1240 °C, monoclinic zirconia turns into tetragonal zirconia with a fluorite-like structure distorted (t-ZrO₂). Here Zr⁴⁺ is surrounded by eight anions, but with two different distances between anions and cations, Zr⁴⁺ - O²⁻. Finally, at 2370 °C, it is transformed into cubic zirconia with fluorite-type structure (F-ZrO₂), with the ion Zr⁴⁺ surrounded by eight anions [2]. It is important phase transformations are reversible during the cooling process.

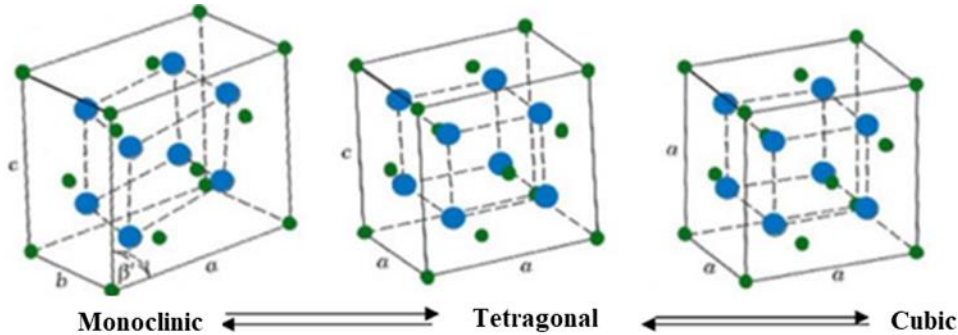


Figure 1: Crystalline phases of pure zirconia (the blue circles represent the ions of O, and the green circles represent the ions of Zr) (Rezaei et al. 2006)

In order to avoid the enormous volume variation observed in the transformation of monoclinic ↔ tetragonal phases (Figure 2), zirconia-based ceramics can be partially or totally stabilized by the incorporation of cations with valences lower than that of Zr⁴⁺, as is the case of alkaline earth cations (for example Mg²⁺ and Ca²⁺) or rare earth cations (such as Y³⁺, Gd³⁺ and Nd³⁺), in order to form solid substitution solutions. Total stabilization means the creation of conditions that allow the cubic phase to be kept at room temperature. Other solutions are also possible involving the coexistence of the tetragonal and cubic phases, commonly called partial stabilization, in which these phases are normally in a metastable condition at room temperature (Muñoz Meneses 2013).

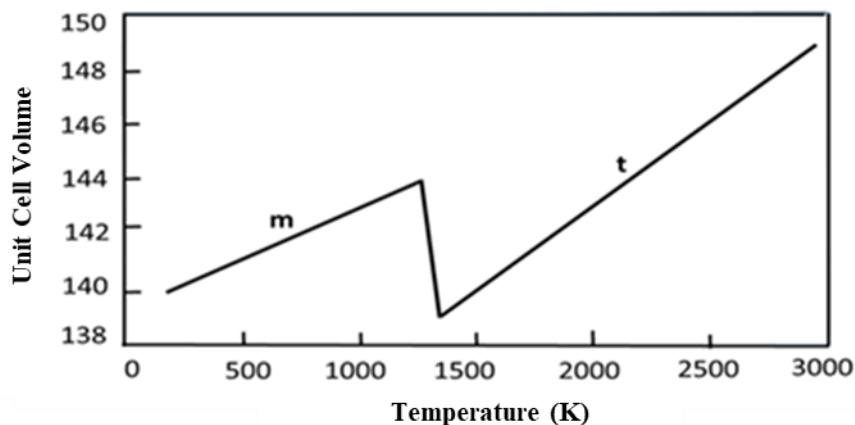


Figure 2: Volume variation of a single zirconia cell during heating / cooling, where m and t are the monoclinic and tetragonal phases (Muñoz Meneses 2013)

The oxide most used for partial or total stabilization of zirconia is yttrium oxide, Y₂O₃, as it confers a considerable beneficial effect on its electrical and mechanical properties, compared to pure zirconia. However, the present work aims to study the partial stabilization of zirconia

with MgO. It is the most frequent solution in the manufacture of oxygen sensors for molten metals. The phase diagram (Figure 3) clearly shows the effect of the addition of MgO on the stability ranges of the three structural forms of zirconia (Muñoz Meneses 2013).

For high temperatures ($> 1750\text{ }^{\circ}\text{C}$), when doping is done with concentrations above 8% (molar), cubic zirconia is obtained. With less than 1-2%, tetragonal zirconia is obtained. Neither phase is stable until room temperature ($20\text{ }^{\circ}\text{C}$). However, between these extremes, an almost stable phase mixture is obtained up to room temperature, known as partially stabilized zirconia or PSZ (Muñoz Meneses 2013). In reality, it is possible to “freeze” the stable high temperature phases as long as the cooling is reasonably fast and it will be in this range of compositions that the present work will focus.

The mastery of the cooling processes of these materials from sintering temperature to room temperature is an essential element in the preservation of these phases, but also in relation to their distribution in microstructural terms, which is also important in terms of properties. This justifies the attention given in this work to the results obtained with materials subject to different cooling speeds.

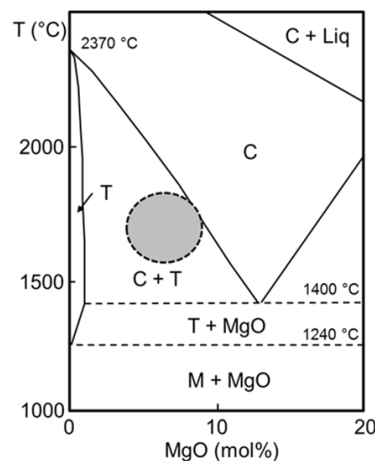


Figure 3: Partial view of the phase diagram $\text{ZrO}_2\text{-MgO}$. The shaded zone identifies the range of compositions and temperatures usual in the manufacture of sensors for molten metals (Muñoz Meneses 2013)

With the stabilization of zirconia with di- and trivalent dopants, the formation of defects also occurs, that is, the formation of anionic gaps occurs in order to maintain electrical neutrality. The gaps are responsible for the mobility of oxygen ions, and consequently, their presence increases ionic conductivity in relation to ZrO_2 in its pure state (Pawłowski, Bućko, and Pędzich 2002). This means that the introduction of dopants manages to achieve the dual purpose of extending the stability domain of the phases of greater symmetry and at the same time promoting large concentrations of ionic defects that allow these materials to behave as solid electrolytes. This last reality is equally important for the application in view in this work.

2.1. Applications of solid electrolytes based on zirconium oxide

The main application of cubic zirconia is in solid electrolytes used in oxygen sensors, SOFC (from Solid Oxide Fuel Cells) and electrochemical pumps (Dunst, Jasinski, and Jasinski 2014). Oxygen sensors are now used in multiple processes that normally involve fossil fuels, a subject that will be detailed later. Fuel cells are electrochemical devices that convert chemical energy in a reaction into electrical energy. Basically, the physical structure of a fuel cell consists of a layer of an electrolyte between an anode and a porous cathode on each side (Fonseca 2001). Electrochemical pumps are less common devices, but with interesting application niches, particularly in oxygen enrichment processes in gas streams. As mentioned, in the present

study special emphasis will be given to the application of solid electrolytes based on zirconium oxide in oxygen sensors for molten metals.

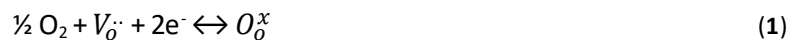
2.2. Oxygen sensors

Oxygen sensors can be classified into two categories depending on the material used:

- Solid electrolyte sensors, consisting of solid ionic conductors, in which the operation is based on electrochemical phenomena.
- Semiconductor sensors, consisting of semiconductor materials and whose operation is based on electronic transport phenomena dependent on surface or volume reactions with the atmosphere.

There is a wide range of electrochemical gas sensors, based on ionic conductive materials. The oxygen sensors are used in the monitoring of oxygen in exhaust gases from automobiles (which allows controlling the air / fuel ratio minimizing the emission of pollutants), or even in the monitoring of oxygen during metallurgical processes allowing a better control of the quality of products (Fonseca 2001).

We can distinguish two main types of electrochemical sensors: potentiometric sensors and amperometric sensors. In both cases the principle of operation is somehow related to the reaction between defects in the solid electrolyte and oxygen in the measurement environment. The predominant defects are the oxygen gaps $V_{O^{\cdot\cdot}}$ and this balance can be described by the Equation (1).



where ions and defects are represented using Kroger-Vink notation.

Potentiometric sensors are galvanic cells that allow quick and direct measurements of concentrations or activities in gases, liquids or melts (Fonseca 2001). The advantages are its portability, ease of automation, the possibility of miniaturization and low cost.

In amperometric sensors, detection is based on the relationship between a limit current that passes through the electrolyte and the concentration of the electroactive species. The limit current depends only on the diffusion of the species to be detected through a diffusion barrier that can be formed by a porous layer deposited on the cathode, or by a small cavity with an opening of approximately 30 μm in diameter surrounding the cathode (Lowinsohn and Bertotti 2006).

Potentiometric oxygen sensors have two electrodes separated by a solid electrolyte. In this type of sensor, the detection is based on the reading of an electromotive force that corresponds to the difference in electrical potential generated by the difference in chemical oxygen potential between the two sides of the sensor (Caproni 2007). The electromotive force, E , is expressed by the Nernst Equation, being valid only for pure electrolytes.

$$E = \left(\frac{RT}{zF}\right) \ln \left(\frac{pO_{2,1}}{pO_{2,2}}\right) \quad (2)$$

In this equation pO_2 is the partial pressure of oxygen in the media 1 of (reference) and 2 (custom medium), R a perfect gas constant (8.31451 J /mol.K), T the absolute operating temperature, z the number of electrons involved in the reaction (for solid zirconia-based electrolytes, $z = 4$), and F the Faraday constant (96484.6 C.mol⁻¹) (Caproni 2007).

Pure electrolyte is one that by definition has an ionic transport number t_i close to 1 (in usual terms > 0.99), being

$$t_i = \frac{\sigma_i}{\sigma_t} \quad (3)$$

where σ_i is the ionic conductivity and σ_t the total conductivity (ionic and electronic).

Potentiometric sensors have two electrodes, the working and the reference electrodes, the latter of which must be sealed, thus hampering the construction of the sensor. However, the operation is relatively simple, when compared to the amperometric sensors since it only involves the measurement of a difference in electrical potential.

Most potentiometric sensors consist of a solid electrolyte in the form of a closed tube at one end, where electrodes are deposited internally and externally, creating a catalytic surface for the transformation of oxygen molecules (O_2) into oxygen ions (O^{2-}).

2.3. Oxygen sensors in the foundry industry

The sensors are used in a wide range of industries, including steelmaking, heat treatments, metal smelting, glass, ceramics, cellulose, paper, automotive and aerospace industries. Monitoring and control of combustion-related emissions is a major process in many of these industries. The great challenge is to develop highly sensitive and selective sensors with stability in aggressive environments ([Lowinsohn and Bertotti 2006](#)).

Currently the most widely used solid electrolyte in the foundry industry for the manufacture of oxygen sensors is ZrO_2 with 7-9 mol% MgO. This range of compositions gives rise to the so-called partially stabilized zirconias, commonly called PSZ. Given the diversity of dopants potentially involved in the formation of this type of materials, the presence of Mg is made explicit by designating these compositions as Mg-PSZ.

The use of an electrolyte at a very high temperature brings with it an inconvenience, which is the presence of electronic conductivity when subjected to means that involve low levels of oxygen ([Lowinsohn and Bertotti 2006](#)). This means that Nernst's law is no longer obeyed. Given that the ionic and electronic conductivities of the monoclinic, tetragonal and cubic phases are different, with the concentration of doping in the latter two being equally influential, the process of optimizing the chemical composition of PSZ is of great importance. Only by adjusting the chemical composition and phases of Mg-PSZ is it possible to obtain a material in which the ionic conductivity is much higher than the electronic one even in reducing conditions and at very high temperature.

When inserting a molten steel oxygen sensor at 1600 °C, a stable signal for 5-10 s is also required, from which the oxygen concentration can be calculated. In practice, the sensor will only survive for a few seconds, so it is a disposable device.

In the measurement process, the Mg-PSZ tube undergoes a violent temperature change. The correct functioning of the sensor depends on the behavior when thermal shock of the tube. Resistance to thermal shock will have to take into account in particular the contraction observed when the monoclinic-tetragonal phase transformation occurs, with increasing temperature ([Caproni 2007](#)). It is possible to manipulate the speed with which this phase transformation occurs by adapting the cooling profile of Mg-PSZ when manufacturing the sensor. With this procedure, the relative importance of the nucleation and phase growth processes can be changed.

Using a sample with 8 mol% MgO as a reference, at a temperature of 1750 °C we will have two phases (about 80% of cubic phase and 20% of tetragonal phase). During cooling, in treatment at 1300 °C, the precipitation of tetragonal particles is verified in a cubic phase grain matrix. These can be in the form of fine particles or larger grains.

In an additional cooling with treatment at 1000 °C, the two types of tetragonal particles will change to the monoclinic phase, forming different types of monoclinic particles, fine and coarse, and may present different behaviors. For example, fine monoclinic particles during

heating can become tetragonal at lower temperatures than predicted in the phase diagram (Van Wijngaarden, Dippenaart, and Van Den Heever 1987).

3. Materials and Methods

This section describes all the prepared materials and reagents used, as well as the method of preparation of compositions studied. Regarding the techniques used throughout the work, a brief theoretical introduction of the operating principles and test conditions is presented. Materials were prepared to be used as electrolytes in oxygen sensors (Table 1), with 6 to 8 mol% MgO, including increments of 0.5 mol% MgO.

Material	Degree of purity (%)	Supplier
Zirconium oxide (< 5µm)	99.0	Aldrich
Magnesium oxide (325 mesh)	99.0	Aldrich

Table 1: List of materials used, degree of purity and supplier

These samples will be called 6 Mg-PSZ, 6.5 Mg-PSZ, 7 Mg-PSZ, 7.5 Mg-PSZ and 8 Mg-PSZ (Table 2). The choice of this range of compositions was based on previous work on this system and information available on literature on ranges of compositions frequently used for sight application (Liu, An, and Qiu 1999). Due to the hygroscopic nature of MgO, care was taken to calcinate it at a temperature of 500 °C for 4 h before proceeding to its dosing in the mixtures. The powders were dosed and weighed on an analytical balance according to the desired composition and were then subjected to dry homogenization in a high energy planetary mill (Retsch PM100), for 45 min, at 250 revolutions per minute (rpm). For this, nylon containers of about 100 cm were used 3 internal volume, and tetragonal zirconia balls with 3 mol% Y₂O₃ (Tosoh Co), in a 10:1 weight to balls / reagents ratio. The grinding comprised a period of 30 effective minutes with pauses of 3 minutes every 5 minutes, in order to cool the vats. The use of high-energy grinding was intended to facilitate the synthesis and sintering of the studied materials.

Acronym	% mol ZrO ₂	% mol MgO
6 Mg-PSZ	94	6
6.5 Mg-PSZ	93.5	6.5
7 Mg-PSZ	93	7
7.5 Mg-PSZ	92.5	7.5
8 Mg-PSZ	92	8

Table 2: Acronyms and compositions of the studied materials

The samples were formed by uniaxial pressing at 10 kN, obtaining cylindrical bodies (inserts) with 10 mm in diameter and about 2 mm in thickness. The mass used for each disc was on average 0.5 grams, with the discs being used for structural, microstructural and electrical characterization. For dilatometry samples, with bar shapes about 12.5 mm long, 2.5 mm wide and 4.4 mm high, the pressure used was 5 kN and the average mass was 0.8 grams. A dimethyl-phthalate-based lubricant was used on the side walls of the die and on the surfaces of the punches in order to reduce friction in the pressing. For each composition, 5 tablets and two bars were prepared, with the dimensions mentioned above.

The sintering temperature for all samples was 1700 °C, with a level of 3 hours. The heating speed for all samples was 3 °C.min⁻¹, but the cooling speed was 1, 2 or 4 °C.min⁻¹, in order to assess the influence of cooling on the phased composition and microstructural development.

The degree of densification of the sintered samples was calculated from the mass and the dimensions (thickness and diameter) of the same in relation to the theoretical density of a “model composite”, obtained from a simple mixing rule of the theoretical densities of the oxide components in the proportions used. Note that there is great uncertainty as to the actual composition of phases (and the composition of each phase) and that it varies for the same composition, but with different cooling rates. Thus, there is no standard theoretical density for each composition, and the values present must be considered only in indicative terms in view of the limitations mentioned.

Using this approximate method, the estimated values for the densification of the samples are between 91 and 96%, as will be indicated in the presentation and discussion of results. Microstructural observation suggests diminutive porosity, corresponding to the densifications equal to or greater than 95%.

Dilatometry is a widely used technique for study of phase transformations since it allows to identify the temperature of these transformations in terms of dimensional changes. With it is still possible to determine the consistency between the phase transformation temperature during heating and cooling, can any differences indicate limitations experimental or kinetic.

For the present work, the BHR horizontal dilatometer, Dil 801L was used. Heating / cooling rates were used in $10\text{ }^{\circ}\text{C}\cdot\text{min}^{-1}$ up to / from $1550\text{ }^{\circ}\text{C}$, and all tests were performed in air. The heating limit temperature was chosen taking into account the limitations of the equipment, but also the ability to access the formation of the cubic phase. Thus, the tests performed should allow identify at monoclinic \leftrightarrow tetragonal transitions and tetragonal \leftrightarrow cubic.

The hardness of a material is defined as its resistance to plastic deformation when subjected to indentation. In the indentation, a load is applied to a material, using points of variable geometry (spherical, conical or pyramidal) made of high hardness materials (steels or diamond), and then the dimensions of the residual impression left on the material are measured after the withdrawal of the indenter (Muccillo, Muccillo, and Saito 1998).

The surface resistance of the dense samples was determined through the Vickers hardness test, using a Shimadzu mechanical indenter. The tests were performed applying a maximum load of 1.5 kgf for 30 s for each measurement. For each sample, 5 measurements were made, with the hardness of each material obtained from the average of these values.

In the present work, Vickers micro-hardness was used. It is based on the resistance that a material offers to the penetration of a diamond pyramid with square base and angle between the faces of 136° , under load (Muccillo, Muccillo, and Saito 1998).

The Vickers microhardness (HV) calculations were made based on the following expression:

$$HV = 1.8544 F/d^2 \tag{4}$$

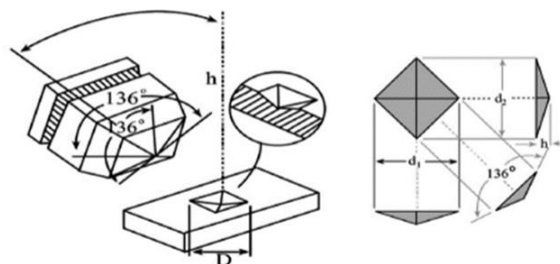


Figure 4: Schematic representation of a Vickers indenter and the brand to be analyzed, including lengths (d_1 and d_2) of the indentation diagonals (Muccillo, Muccillo, and Saito 1998)

X-ray diffraction is one of the most important and most powerful techniques for characterizing materials. This technique is based on X-ray diffraction through the planes of atoms or ions. X-ray wavelengths are like interatomic distances ($\lambda \approx 1\text{\AA}$).

The interaction of radiation with the sample can take different forms. For crystalline samples, the diffraction phenomenon can give rise to constructive interference phenomena for different incident angles. The measurement of these allows the determination of the distance between the atoms / ions in the crystal and, from these, the identification of the crystalline structure. The relationship between the X-ray wavelength (λ), the interplanar distance for the set of planes (d) and the angle of incidence (θ) is described by Bragg's law:

$$2d \sin \theta = n\lambda \tag{5}$$

where n is an integer. The analysis of diffractograms usually focuses on the number of peaks, intensity and position, constituting specific and unique characteristics of each crystalline substance (Muccillo, Muccillo, and Saito 1998; Meynen, Cool, and Vansant 2009).

Scanning electron microscopy (SEM) is used to study the morphology and topography of materials up to a sub-micrometric scale. The surface under study is scanned sequentially (sweeping) by an electronic beam with high kinetic energy, producing several signals, namely secondary, retro-diffused electrons, X-rays and Auger electrons. The detection of these signals allows you to create images with topography and chemical composition information (atomic number) provided the appropriate detectors are available (Meynen, Cool, and Vansant 2009). The samples were observed by scanning electron microscopy, on a Hitachi SU-70 microscope, equipped with a Rontec energy dispersion detector, to allow an identification of the distribution and composition of the phases present. The preparation of the samples was done without polishing, being only glued on an aluminum support, later covered with carbon film, by sputtering.

4. Discussion

Figure 5 and Figure 6 show the X-ray diffractograms of the sintered samples (with identification of the monoclinic, tetragonal and cubic phases) and corresponding powders (with identification of the monoclinic, tetragonal and cubic phases) obtained by grinding, all cooled to $1\text{ }^\circ\text{C}\cdot\text{min}^{-1}$.

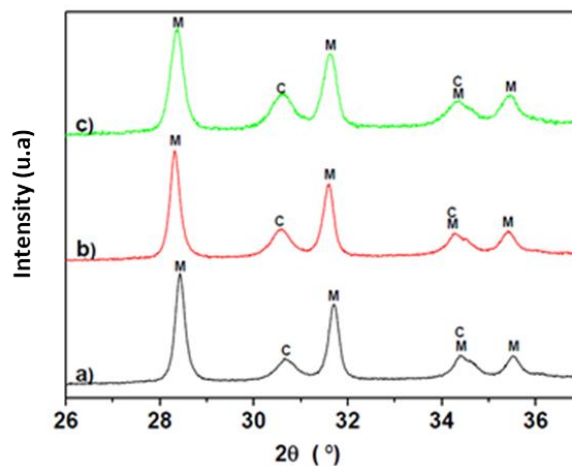


Figure 5: XRD of the powder of different samples cooled to $1\text{ }^\circ\text{C}\cdot\text{min}^{-1}$: (a) 6 Mg-PSZ; (b) 6.5 Mg-PSZ and (c) 7 Mg-PSZ

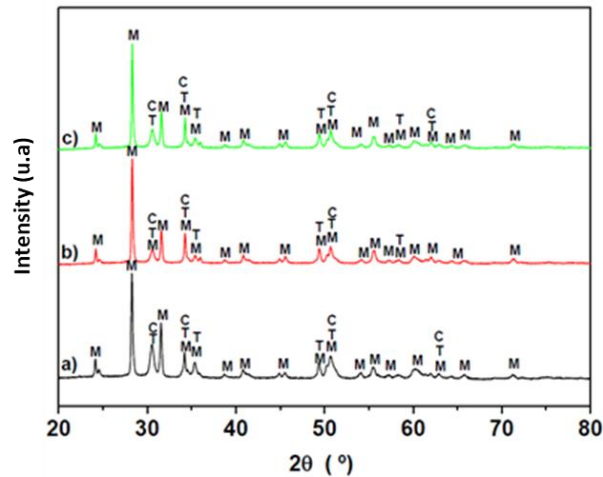


Figure 6: XRD of different samples (dense) after cooling to $1\text{ }^{\circ}\text{C}\cdot\text{min}^{-1}$: (a) 6 Mg-PSZ, (b) 6.5 Mg-PSZ and (c) 7 Mg-PSZ

In addition to the constraints associated with an XRD analysis of a sintered sample, in this case, there is an overlap between the main peaks of the tetragonal and cubic phases. These problems are difficult to solve and are already known in the literature. However, with the grinding of the sintered samples, an evaluation of the content in the cubic phase is achieved. Thus, although the two sets of results presented do not provide the desirable information on the composition of phases, together they allow a complementary image of the materials obtained.

Regarding [Figure 5](#) and [Figure 6](#), in samples with a low amount of magnesium (6 Mg-PSZ) the predominance of the monoclinic phase is observed in relation to the other phases. In samples with a high amount of magnesium (7 Mg-PSZ) the cubic phase predominates, which was to be expected since the amount of dopant increases.

The increase in the percentage of MgO favors the formation of high concentrations of cubic phase during sintering, as can be concluded from the analysis of the phase diagram. However, during slow cooling from the sintering temperature, the conversion of the cubic to tetragonal phase causes the increase in the MgO content of the cubic phase simultaneously with the decrease of the relative percentage of the cubic phase. Finally, the conversion of the tetragonal phase to monoclinic at lower temperatures explains the relative importance of the peaks in these phases.

[Figure 7](#) shows the results of the microstructural characterization of samples prepared in this work. [Figure 7](#) refers to the 7 Mg-PSZ sample obtained at different cooling rates. Analyzing this figure, one can notice the presence of small particles (in black) that correspond to MgO and tend to disappear with an increase in the cooling speed (a, c and e). The large grains should be cubic and the small ones monoclinic.

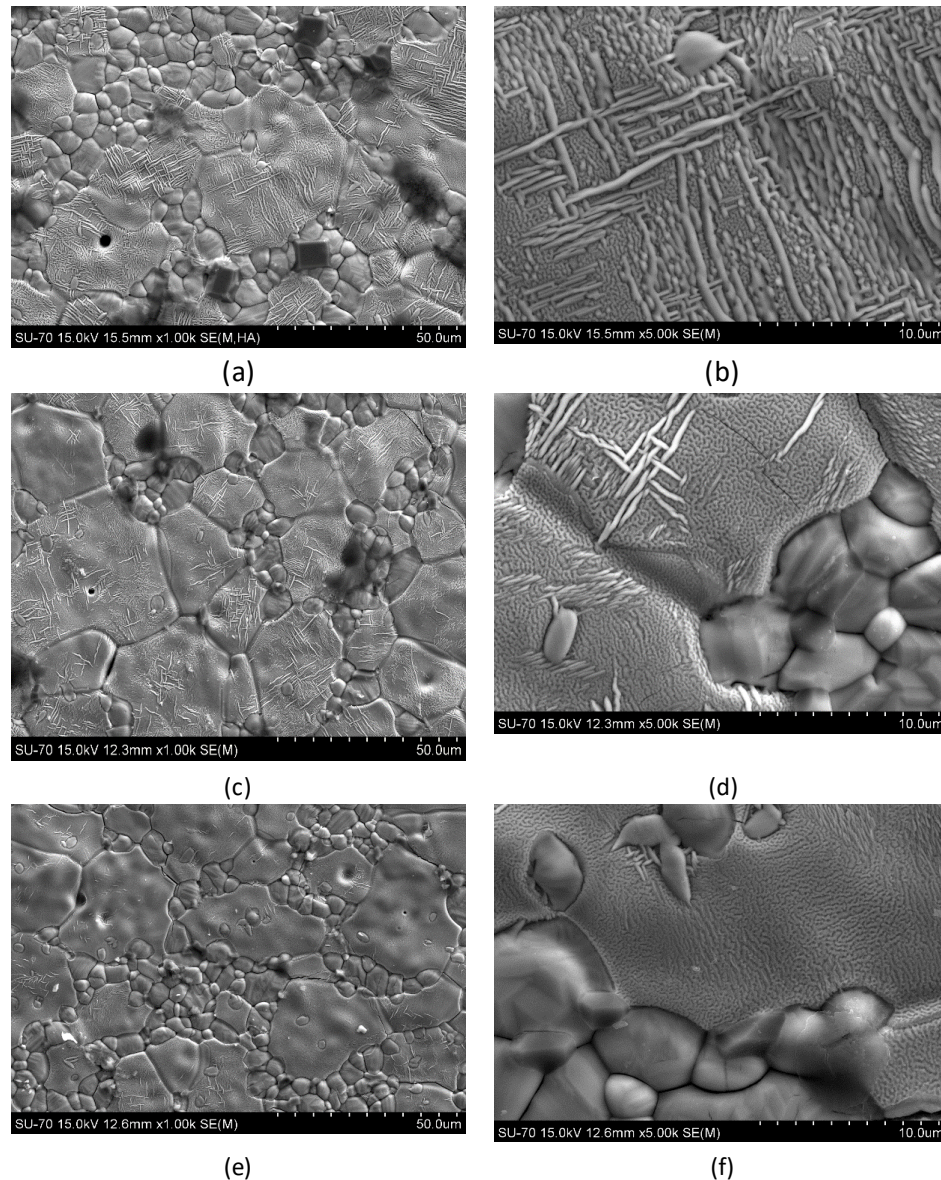


Figure 7: Microstructures under various enlargements (1000 and 5000 x) of the 7 Mg-PSZ samples obtained with different cooling speeds: (a and b) - 1 °C.min⁻¹; (c and d) - 2 °C.min⁻¹; (e and f) - 4 °C.min⁻¹

Figure 8, Figure 9, and Figure 10 show the results of dilatometric analyzes with different cooling rates (1 °C.min⁻¹ - 6; 6.5 and 7 Mg-PSZ, 2 °C.min⁻¹ - 6; 6.5; 7; 7.5 and 8 Mg-PSZ, and 4 °C.min⁻¹ - 6; 6.5 and 7 Mg-PSZ). In general, the samples with the three cooling speeds exhibit similar behavior from 300 °C to 1100 °C, however, it is distinguished by the slight variation in behavior close to 800 °C, visible for samples with cooling of 2 °C.min⁻¹ and 4 °C.min⁻¹. This behavior, which causes a reduction in the average expansion coefficient in this temperature range, is due to the conversion of small particles (needles) of monoclinic zirconia dispersed in the cubic matrix into tetragonal zirconia, below the expected phase transition temperature. A little above 1100 °C there is a sharp variation in the samples with cooling of 1 °C.min⁻¹ as a result of the transformation of the (small) grains of monoclinic zirconia into tetragonal. Note that the amplitude of this transformation is conditioned by the cooling speed, being maximum for the samples with the lowest cooling speed, where the presence of a monoclinic phase in small grains is also maximum and the presence of small particles dispersed in the cubic phase

is minimal. The expansion then proceeds evenly up to 1500 °C, with a slight change in slope near the transition between the tetragonal and cubic phases (just above 1400 °C).

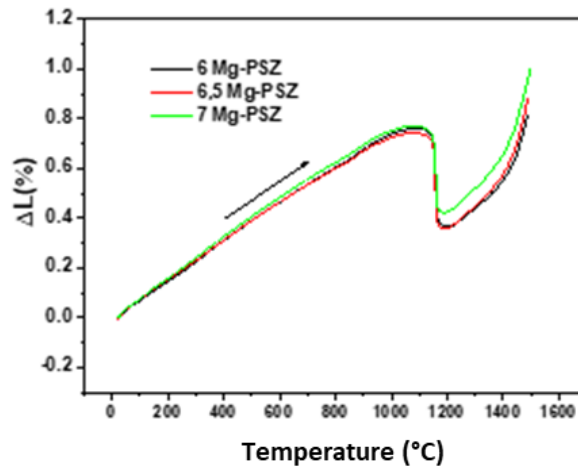


Figure 8: Dilatometric analysis of the samples obtained with a cooling speed of 1 °C.min⁻¹

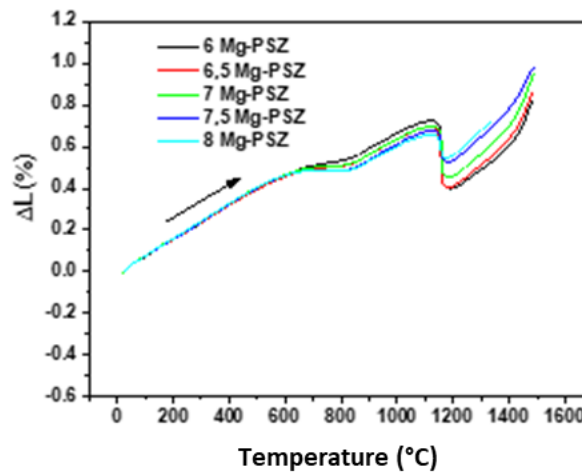


Figure 9: Dilatometric analysis of the samples obtained with cooling speeds of 2 °C.min⁻¹

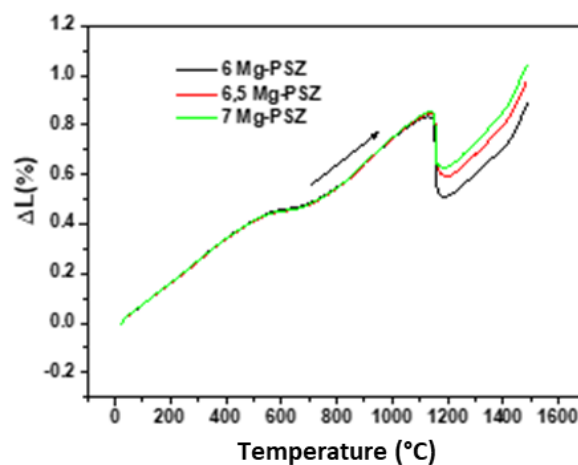


Figure 10: Dilatometric analysis of the samples obtained with a cooling speed of 4 °C.min⁻¹

Figure 11 shows the air impedance spectra of 6.5 Mg-PSZ at different temperatures (525 °C and 800 °C) and with different cooling speeds. At low temperatures (Figure 11a) it is possible

to observe the existence of arcs with marked depression, suggesting the existence of a minimum of two contributions in the higher frequency ranges. For the sample subject to a lower cooling speed, the presence of two arcs is clear. It should be remembered that the coexistence of phases and the complexity of the microstructures does not allow a simple identification of these arcs with a grain or grain boundary behavior, although it is always assumed that the highest frequency behavior is related to transport within grains (possibly from the cubic phase, more conductive) while the lower frequency behavior will be influenced by the grain boundaries of the more conductive phase but also by the presence of dispersed insulating phases such as monoclinic. The low frequency tail, usually related to the electrode process, is not visible in low temperature spectra.

The relative magnitude of the impedances of the samples at low temperature indicates that the increase in the cooling speed allows the phase of greater symmetry and conductivity (cubic) to be frozen, thus increasing the overall conductivity of these materials. The monoclinic phase, insulating in comparison with the cubic and tetragonal phases, promotes an increase in the blocking of the transport of oxygen ions, increasing the electrical resistivity. Although in a qualitative way, the amplitudes of the spectra now analyzed show that the simple manipulation of the cooling speed allows to obtain conductivity values differing by a factor of 2, a manifestly unusual situation in the field of solid ceramic electrolytes.

At high temperatures (Figure 11b) it is possible to observe a slight low frequency tail corresponding to the so-called electrode arc, while any resolution between arcs related to the behavior of Mg-PSZ is lost. This is a normal situation in terms of impedance spectroscopy, which is why it is only possible to extract total resistance values for the material under study. Higher conductivity is confirmed again for the sample subjected to the higher cooling rate.

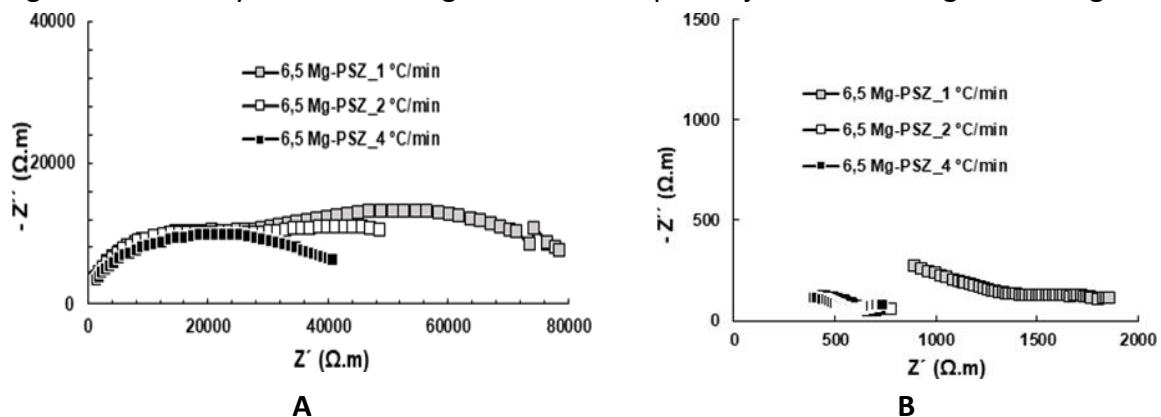


Figure 11: Air impedance spectra (corrected for sample dimensions) obtained for 6.5 Mg-PSZ with different cooling speeds: (A) 525 °C; (B) 800 °C

5. Conclusions

The present work allowed us to draw a set of important conclusions about the relationships between the composition, processing and behavior of different materials in the zirconia-magnesia system. Among these we can highlight:

- the adjustment of Mg content and cooling cycles contributes to a profound change in the composition of phases, but also in their distribution in microstructural terms, being really key in terms of the thermal behavior of this material;
- it is clearly possible to improve the electrical conductivity of these materials by manipulating (increasing) the cooling speed and doping concentration, without considering that any of these effects clearly prevails in relation to the other;

- the existence of large concentrations of monoclinic phase grains gives rise to materials exhibiting large dimensional variations in a short range of temperatures, less resistant to thermal shock;
- the controlled precipitation of fine particles of tetragonal phase within the cubic matrix and subsequent conversion to a monoclinic phase is crucial in the development of materials with excellent resistance to thermal shock.

The work carried out also has different limitations that leave open the possibility that they will be resolved in future work. The following stand out:

- microstructural analyzes should evolve towards quantification (what percentages of phases, what particle dimensions and what location) so that the desirable quantitative relationships with thermal and electrical behavior can be established;
- the hardness measurements justify a repetition of the tests carried out in order to confirm or review the type of observed trends, thus allowing to draw conclusions that at the moment seem unsustainable;
- the performance of tests of thermal shock and electrochemical behavior in conditions similar to those verified in industrial sensors is essential so that the conclusions of the work carried out can be fully confirmed.

References

- Caproni, É. 2007. "Estudo de eletrólitos sólidos cerâmicos à base de óxido de zircônio para a detecção de oxigênio". PhD diss., Instituto de Pesquisas Energéticas e Nucleares - IPEN/CNEN-SP, São Paulo. <https://doi.org/10.11606/T.85.2007.tde-30032012-101612>.
- Dunst, K., G. Jasinski, and P. Jasinski. 2014. "Potentiometric oxygen sensor with solid state reference electrode". *Metrology and Measurement Systems* 21, no. 2: 205-16. <https://doi.org/10.2478/mms-2014-0018>.
- Fonseca, F. C. 2001. "Relação microestrutura - propriedades elétricas de compósitos cerâmicos à base de zircônia". PhD diss., Instituto de Pesquisas Energéticas e Nucleares - IPEN/CNEN-SP, São Paulo. <http://repositorio.ipen.br/handle/123456789/10906>.
- Grzebielucka, E. C., A. S. A. Chinelatto, S. M. Tebcherani, and A. L. Chinelatto. 2010. "Synthesis and sintering of Y2O3-doped ZrO2 powders using two Pechini-type gel routes". *Ceramics International* 36, no. 5 (july): 1737-42. <https://doi.org/10.1016/j.ceramint.2010.02.042>.
- Liu, Q., S. An, and W. Qiu. 1999. "Study on thermal expansion and thermal shock resistance of MgO-PSZ". *Solid State Ionics* 121, no. 1-4 (june): 61-65. [https://doi.org/10.1016/S0167-2738\(98\)00529-3](https://doi.org/10.1016/S0167-2738(98)00529-3).
- Lowinsohn, D., and M. Bertotti. 2006. "Sensores eletroquímicos: Considerações sobre mecanismos de funcionamento e aplicações no monitoramento de espécies químicas em ambientes microscópicos". *Química Nova* 29, no. 6: 1318-25. <https://doi.org/10.1590/S0100-40422006000600029>.
- Muñoz Meneses, R. A. 2013. "Microestrutura e propriedades elétricas da zircônia dopada com óxidos mistos de terras raras para aplicação como eletrólito sólido em sensores de oxigênio". PhD diss., Universidade de Brasília. <https://repositorio.unb.br/handle/10482/15202>.
- Meynen, V., P. Cool, and E. F. Vansant. 2009. "Verified syntheses of mesoporous materials". *Microporous and Mesoporous Materials* 125, no. 3 (october): 170-223. <https://doi.org/10.1016/j.micromeso.2009.03.046>.

- Muccillo, R., E. N. S. Muccillo, and N. H. Saito. 1998. "Thermal shock behavior of ZrO₂:MgO solid electrolytes". *Materials Letters* 34, no. 3-6 (march): 128-32. [https://doi.org/10.1016/S0167-577X\(97\)00152-3](https://doi.org/10.1016/S0167-577X(97)00152-3).
- Pawłowski, A., M. M. Bućko, and Z. Pędzich. 2002. "Microstructure evolution and electrical properties of yttria and magnesia stabilized zirconia". *Materials Research Bulletin* 37, no. 3 (march): 425-38. [https://doi.org/10.1016/S0025-5408\(01\)00816-9](https://doi.org/10.1016/S0025-5408(01)00816-9).
- Rezaei, M., S. M. Alavi, S. Sahebdehfar, and Z.-F. Yan. 2006. "Tetragonal nanocrystalline zirconia powder with high surface area and mesoporous structure". *Powder Technology* 168, no. 2 (october): 59-63. <https://doi.org/10.1016/j.powtec.2006.07.008>.
- Van Wijngaarden, M. J. U. T., R. J. Dippenaar, and P. M. Van Den Heever. 1987. "An evaluation of the electrochemical oxygen probes used in steelmaking". *Journal of the Southern African Institute of Mining and Metallurgy* 87, no. 9 (september): 269-78. <https://www.saimm.co.za/journal-papers/details/1/1125>.